Petroleum Science 19 (2022) 2150–2164

Contents lists available at ScienceDirect

Petroleum Science

journal homepage: www.keaipublishing.com/en/journals/petroleum-science

Original Paper

Double network self-healing hydrogel based on hydrophobic association and ionic bond for formation plugging

Ying-Rui Bai [a], Qi-Tao Zhang [a], Jin-Sheng Sun [a, b, *], Guan-Cheng Jiang [c], Kai-He Lv [a]

[a] School of Petroleum Engineering, China University of Petroleum (East China), Qingdao, 266580, Shandong, China
[b] CNPC Engineering Technology R&D Company Limited, Beijing, 102206, China
[c] College of Petroleum Engineering, China University of Petroleum (Beijing), Beijing, 102249, China

ARTICLE INFO

Article history:
Received 1 May 2022
Received in revised form
18 July 2022
Accepted 20 July 2022
Available online 31 July 2022

Handling Editor: Jian-Chao Cai
Edited by Yan-Hua Sun

Keywords:
Self-healing hydrogel
Hydrophobic association
Ionic bond
Mechanical property
Rheological property
Formation plugging

ABSTRACT

Self-healing hydrogels have attracted tremendous attention in the field of oil and gas drilling and production engineering because of their excellent self-healing performance after physical damage. In this study, a series of double network self-healing (DN_{SA}) hydrogels based on hydrophobic association and ionic bond were prepared for plugging pores and fractures in formations in oil and gas drilling and production engineering. The mechanical, rheological, and self-healing properties of the DN_{SA} hydrogels were investigated. Results revealed that the DN_{SA} hydrogels exhibited excellent mechanical properties with a tensile stress of 0.67 MPa and toughness of 7069 kJ/cm^3 owing to the synergistic effect of the double network. In addition, the DN_{SA} hydrogels exhibited excellent compression resistance, notch insensitivity, and self-healing properties. The DN_{SA}-2 hydrogel was granulated and made into gel particles with different particle sizes and used as a plugging agent. The self-healing mechanism of DN_{SA}-2 hydrogel particles in fractures was explored, and it's plugging effect on fractures of different widths and porous media of different permeabilities were investigated. Experimental results revealed that the plugging capacity of the DN_{SA}-2 hydrogel particles for a fracture with width of 5 mm and a porous medium with a permeability of 30 μm^2 was 3.45 and 4.21 MPa, respectively, which is significantly higher than those of commonly used plugging agents in the oilfield. The DN_{SA} hydrogels with excellent mechanical and self-healing properties prepared in this study will provide a new approach for applying hydrogels in oil and gas drilling and production engineering.

1. Introduction

Hydrogels are soft substances formed by chains of hydrophilic macromolecules linked together in a chemical or physical cross-linking process. It is a soft material with a three-dimensional network structure, which tends to lock in a large amount of water due to a large number of hydrophilic groups in the network chains (Sun et al., 2012; Unagolla and Jayasuriya, 2020). Owing to their adjustable properties and unique intelligent characteristics (e.g., pH responsiveness (Bazban-Shotorbani et al., 2017; Qu et al., 2017)), thermal responsiveness (Hao et al., 2013; Xue et al., 2018), self-healing properties (Taylor and In Het Panhuis, 2016; Yu et al., 2014), and shape memory capability (Lu et al., 2017; Xiao et al., 2017)), hydrogels have been widely used in industrial, agricultural, and medical fields (e.g., flexible devices (Zhang et al., 2021), 3D printing (Ouyang et al., 2016; Yuan et al., 2022; Li et al., 2018), adsorbents (Shah et al., 2018), and drug release carriers (Hamidi et al., 2008; Webber et al., 2015)). Effective energy dissipation systems allow the forces on the hydrogels to be distributed appropriately, thus optimizing the toughness and strength of the hydrogels (Koetting et al., 2015). However, the lack of an effective energy dissipation mechanism in conventional hydrogels has resulted in poor mechanical properties and toughness, which significantly limit the application of hydrogels in practical production. To optimize the properties of hydrogels, researchers have devoted tremendous efforts to explore reasonable energy dissipation systems. Presently, hydrogels with excellent energy dissipation capabilities include double network (DN) hydrogels (He et al., 2021; Zhang et al., 2016), nanocomposite hydrogels (Gaharwar et al.,

* Corresponding author. School of Petroleum Engineering, China University of Petroleum (East China), Qingdao, 266580, Shandong, China.
E-mail address: sunjsdri@cnpc.com.cn (J.-S. Sun).

https://doi.org/10.1016/j.petsci.2022.07.006

2014; Merino et al., 2015), slide-ring hydrogels (Liu et al., 2021), and microgel-reinforced hydrogels (Hu et al., 2020; Zheng et al., 2015), etc.

The concept of DN hydrogels was first introduced by Gong et al., in 2003 (Gong et al., 2003), and they exhibit a unique energy dissipation mechanism that endows them with excellent mechanical properties and toughness. The rigid and brittle first layer network acts as a reversible sacrificial bond, thus effectively dissipating energy, and the soft second layer network acts as a permanent cross-link that endows the hydrogel with gel elasticity and greater stress. However, the first layer of the conventional DN hydrogels is mostly composed of irreversibly rigid covalent bonds, which damage the rigid and brittle first layer when impacted by external force, thus significantly weakening the recovery performance and fatigue resistance of the hydrogels. Therefore, researchers have attempted to replace the first layer of the network with a reversible non-covalent bond to avoid the defects of the rigid chemical bond and optimize the fatigue resistance and healing ability of hydrogels. Accordingly, Zhang et al. (2016) reported a new fully physically cross-linked DN hydrogel, which contains a strong hydrophobic association cross-linked amphiphilic triblock copolymer network and a polyacrylamide (PAAm) network. In addition, the hydrogel was composed of hydrogen bonds between the two layers of the network as sacrificial bonds. Consequently, this hydrogel exhibited a good tensile strength and good toughness; however, the preparation process is too complicated and the organic solvent used is not sufficiently friendly to the environment.

The self-healing properties of hydrogels are extremely attractive. Self-healing gels can heal autonomously using covalent bonds (acylhydrazone bonds (Liu et al., 2020), DA reactions (Saghafi et al., 2016; Scheltjens et al., 2013), and imine bonds (Xu et al., 2018)) and non-covalent bonds (hydrogen bonds (Zhao et al., 2021), hydrophobic association (Tuncaboylu et al., 2012), and ionic bonds (Zhong et al., 2015)) under suitable temperature conditions without relying on external forces. Among them, hydrophobic linkage exhibits excellent self-healing effect. Tuncaboylu et al. (2011, 2012) prepared a hydrophobic linkage hydrogel by introducing hydrophobic groups into the polymer molecular chain, and the hydrogel exhibited a very high healing performance (100%) and elongation (3600%), but the fracture stress of the hydrogel was less than 100 kPa. Double network hydrogels tend to exhibit better healing and recovery properties than single network hydrogels due to their unique energy dissipation system. Ionic bonds have attracted extensive research attention owing to their good thermal stability and kinetic instability. Sodium alginate (SA) is widely used in the production of hydrogels owing to the presence of carboxyl groups, which can be coordinated with metal ions of different valency (e.g., Ca^{2+}, Sr^{2+}, Fe^{3+}) (Yang et al., 2013). Sun et al. (2012) designed hybrid interpenetrating polymers using ionic cross-linked SA and covalently cross-linked PAAm. The composite hydrogels exhibited good toughness and recovery at 80 °C, but the tensile strength was only 160 kPa, and the formation of most of the ionic bonds was mostly dependent on immersion, which is not conducive for large-scale production.

Because of their excellent mechanical properties and deformable performance, hydrogels are widely used in oil and gas drilling and production engineering. In addition, they are often used as plugging agents and lost circulation materials (Jiang et al., 2019; Larki et al., 2019; Mansour and Taleghani, 2018) during drilling process and the oil recovery process as profile control agents and water shutoff agents (Amir et al., 2019; Kang et al., 2021). Depending on their cross-linking methods, hydrogels used in oil and gas drilling and production engineering are divided into two main categories: preformed particle gels and *in-situ* formed gels. *In-situ* formed gels exhibit a good temperature resistance and high gel strength (Webber et al., 2015), and *in-situ* formed hydrogels based on acrylamide (AM) and chromium cross-linkers exhibit a plugging capacity of more than 1000 psi for fractures with a width of 5 mm after gel formation. El-Karsani et al. (2014) prepared an *in-situ* formed gel system based on polyacrylamide/polyethyleneimine (PAAM/PEI), and the gel system maintained its stability at 150 °C with a storage modulus of up to 1087 Pa. However, underground cross-linked gels are susceptible to the shear action of formation pores and fractures, chromatographic separation effect between gel components, and other factors during the migration process, which result in a significant decrease in their gel-forming strength, and difficulties in achieving the high-strength plugging effect in deep formations. These problems can be solved using preformed particle gels (Bai et al., 2007; Li H. et al., 2019). For example, Bai et al. (2013) prepared a preformed particle gel (particle size from 50 μm to 5 mm) using both a stable cross-linker and an unstable cross-linker. After forming a plugging in large pores in the formation, the preformed particle gel can turn into a viscous colloid that can penetrate micro-pores with a permeability of less than 400 mD under high temperature, which is important for improving the waterflood sweep efficiency. However, the strength of the plugging layer of preformed particle gels, which relies solely on inter-particle bridging and filling, is low, thus hindering the achievement of a high strength and effective plugging of large-scale pores and fractures.

As a hydrogel plugging agent, the nature of the hydrogel required for application in different scenarios varies greatly. For example, as a lost circulation material in the drilling process, the hydrogel must have high strength to achieve high strength plugging of large fractures (Jiang et al., 2021). As a water shutoff (Soka and Sidiq, 2022) or profile control agent (Bai et al., 2013), the hydrogel must have good deformability to achieve the purpose of deep-seated plugging. We believe that as a good plugging agent, it must have both good deformability and strength to adapt to the plugging of different types of strata. If the hydrogel plugging agent is self-healing, its plugging performance will be significantly optimized. In recent years, self-healing gels have attracted increasing attention in oil and gas drilling engineering. Self-healing gels can be made into preformed particle gels, which can be used as profile control agents, water shutoff agents, or lost circulation control agents. Self-healing hydrogel plugging agents have the advantages of both traditional preformed particle gels and *in-situ* formed gels. After the gel particles accumulate and fill in the formation pores and fractures, they can heal and form a solid gel with good strength to optimize the plugging effect (Bai et al., 2021). Wang et al. (2017) designed a re-crosslinkable preformed particle gel based on reversible ionic bonding, and the gel heals in brine with 10 wt% NaCl with a storage modulus of up to 10 kPa, and the re-crosslinkable bulk gel formed could significantly reduce the permeability of large fractures. Pu et al. (2019) prepared a self-healing gel profile control agent for low-temperature reservoirs using (acrylamide-acrylic acid) copolymers with a pre-embedded second cross-linker, which exhibits a pressure-bearing capacity of 300 psi/ft within a 2-mm fracture and obtained good results when applied in the field on the North Slope of Alaska.

In this study, we prepared double network self-healing (DN_{SA}) hydrogels based on a fully physically cross-linked DN with combined hydrophobic association and ionic bonding. The hydrophobic association was formed by the simple micellar copolymerization of hydrophobic monomer (lauryl methacrylate (LMA)) and hydrophilic monomer (AM), and the ionic bonding between SA and Fe^{3+} was formed by coordination, and there were also hydrogen bonds between the bilayer network as sacrificial bond, the DN formed by both hydrophobic association and ionic bonding significantly optimized the mechanical strength and toughness of the DN_{SA}

hydrogels. The hydrogels exhibited good fatigue resistance and healing ability owing to the fact that the two layers of networks were composed of non-covalent bonds. We investigated the microscopic morphology, mechanical properties, recovery properties, and rheological properties of the DN_{SA} hydrogels in detail to determine the cross-linking reaction mechanism of the hydrogels. In addition, self-healing preformed particle gels were prepared using the hydrogels, and their pressure-bearing plugging effects on porous media with different permeabilities and fractures of different scales were investigated. This work proves that DN_{SA} hydrogels can be used for formation plugging in oil and gas drilling process.

2. Experimental

2.1. Materials

Sodium alginate (SA, purity≥90%), sodium dodecyl sulfate (SDS, ≥98%), and lauryl methacrylate (LMA, purity 96%) were purchased from Aladdin Chemical Co., LTD. Ferric chloride hexahydrate ($FeCl_3 \cdot 6H_2O$, purity≥99%) and acrylamide (AM, purity≥99%) were purchased from Macklin Biochemical Co., LTD. Ammonium persulfate (APS, purity≥99%) and sodium chloride (NaCl, purity≥99.5%) were purchased from Sinopharm Chemical Reagent Co., LTD.

2.2. Hydrogel preparation

SA significantly affects the mechanical properties of hydrogels. In this study, double network (DN) hydrogels with different concentrations of SA were prepared. The DN_{SA} hydrogels based on hydrophobic association and ionic bonding were prepared using the following: first, 0.36 g of $FeCl_3 \cdot 6H_2O$ was added to 10 mL of deionized water under sufficient stirring to obtain a homogeneous solution. Subsequently, 1 mL of the $FeCl_3 \cdot 6H_2O$ solution was added to SDS (18g) and the mixture was stirred vigorously at room temperature until the solution became a homogeneous clear yellow solution. Thereafter, the mixed solution was heated to 45 °C in a water bath, after which AM (4 g) and LMA (0.12 g) were introduced into the solution and stirred for 1 h at 45 °C. Subsequently, the solution was cooled to 25 °C, after which APS (0.04 g) was added to the solution, and the mixture was quickly degassed in an inert atmosphere. After degassing, the solution was transferred to a homemade square mold (50 mm in length and width, 2 mm in thickness), and lastly, the mold was placed in an oven at 60 °C for 12 h to complete the polymerization process. The detailed recipe and code are shown in Table 1.

2.3. Characterization

The prepared hydrogels were frozen at −20 °C for 24 h. The obtained freeze-dried samples were cut into small pieces and sprayed with gold on fresh sections. The microscopic morphology of the hydrogel samples was observed using a scanning electron microscope (SEM).

Transmittance Fourier transform infrared (FTIR) spectra (PerkinElmer Frontier) of the hydrogels were collected in the range of 4000–550 cm^{-1} with 1 cm^{-1} resolution and eight scans. Before the measurement, the hydrogel samples were soaked in a large amount of deionized water for 48 h (deionized water was replaced every 8 h) to remove the mobile ions and unreacted parts from the hydrogel. Subsequently, the dialyzed hydrogel samples were lyophilized, ground into powder, and pressed with potassium bromide.

The swelling performance of the hydrogels was characterized using the differential method. First, the prepared hydrogel sample was dried at 70 °C to a constant weight, and the mass at this time was denoted as m_1. The prepared dried hydrogel sample was placed in excess deionized water at 25 °C, and the hydrogel mass after swelling was denoted as m_2. The swelling ratio of hydrogel was represented as $(m_2 - m_1)/m_1 \times 100\%$. In this study, the swelling ratio of hydrogels was recorded at different moments during seven days.

2.4. Mechanical tests

Tensile tests were performed on the hydrogels using a universal electromechanical tester (WDW-05, SANS Inc., China) with a load cell of 50 N. The square hydrogels prepared in the mold were cut into dumbbell-shaped samples (2 mm × 2 mm × 30 mm) using a cutter for tensile testing. In this study, uniaxial tensile experiments were conducted on the hydrogel samples at a speed of 50 mm/min. To avoid water loss in the hydrogel samples during the tensile process, each dumbbell-shaped hydrogel sample was coated with a thin layer of silicone oil, and the stress–strain curves were investigated. Young's modulus of the hydrogel sample was determined using the slope of the linear part of the stress–strain curve (strain <20%). The toughness of the hydrogel sample was determined using the integrated area of the stress–strain curve obtained from the tensile test. To clarify the energy dissipation mechanism of the hydrogels, loading–unloading experiments were also performed on the hydrogel samples at loading and unloading speeds of 50 mm/min. The dissipation was obtained using the difference between the integration of the stress–strain curves obtained during the loading process and the stress–strain curves obtained during the unloading process.

Compression tests were performed on the hydrogels using a testing machine (CMT6103, MTS, China) with a 500 N load cell at room temperature. The samples were cut into 10 mm (Φ10 mm). Each hydrogel sample was coated with a thin layer of silicone oil to prevent water loss, and the tests were conducted at a constant speed of 2 mm/min.

Each hydrogel sample was tested at least three times to ensure data accuracy.

2.5. Rheological tests

Rheological tests of the hydrogel samples were performed using a HARKE MARS 60 rotational rheometer, and gel samples with a thickness of 1 mm were clamped using a plate fixture (35-mm diameter plate). The dynamic strain sweeps (γ = 0.1%–1000%) were performed on the hydrogel samples at a fixed frequency (6.28 rad/s) under 25 °C. Strain sweeps determined the transition point and linear viscoelastic region of the gel samples. Subsequently, the frequency sweeps were performed on the hydrogel samples at a fixed strain (1%, within the linear viscoelastic region) with a change in the frequency from 0.1 to 100 rad/s. The fixed-strain and fixed-frequency time sweeps were performed at 25 °C

Table 1
Components for preparing double network self-healing (DN_{SA}) hydrogels.

Hydrogel	Component, g							
	SA	LMA	H_2O	NaCl	SDS	$Fecl_3 \cdot 6h_2O$	AM	APS
SN-1	0.00	0.43	18	0.95	1.26	0	4	0.04
DN_{SA}-1	0.12	0.43	18	0.95	1.26	0.036	4	0.04
DN_{SA}-2	0.24	0.43	18	0.95	1.26	0.036	4	0.04
DN_{SA}-3	0.36	0.43	18	0.95	1.26	0.036	4	0.04
DN_{SA}-4	0.48	0.43	18	0.95	1.26	0.036	4	0.04

($t = 3600$ s, $\gamma = 1\%$, $f = 1$ Hz) to verify the stability of the hydrogels. In addition, the variable strain time sweeps ($\gamma_{min} = 0.1\%$, $\gamma_{max} = 400\%$, $t = 30$ s) were performed at 25 °C to verify the ability of the hydrogel to recover its original properties.

Each set of the above rheological performance tests was repeated at least three times to ensure the accuracy of the data.

2.6. Self-healing experiments

For this analysis, two gel sample strips (one of which was stained with methylene blue) were prepared, and a layer of water was applied to an incision without any external force. The two gel strips were placed in a sealed bag with cross-sectional contact, after which they were placed in an oven and heated at 70 °C for 12 h (Target application temperature of gel plugging agent). The fracture stress of the original hydrogel samples was defined as σ_0, and the fracture stress of the healed hydrogel samples was defined as σ_1. The healing efficiency was defined as the ratio of the fracture stress of the healed gel samples to the fracture stress of the original gel samples (i.e., $\sigma_1/\sigma_0 \times 100\%$). Each hydrogel sample was tested at least three times to ensure data accuracy.

2.7. Plugging tests

According to the "1/2″ bridging theory, self-healing hydrogel particles with particle size matching the fracture width and pore diameter were selected and prepared into a dispersion with a concentration of 3%. For the fracture plugging experiments, the dispersion liquid containing self-healing hydrogel particles was injected into fracture cores with a width of 0.5–5.0 mm and a length of 50 cm, and the real-time injection pressure at the fracture entry section was recorded. After the injection pressure was stabilized, the injection of the hydrogel was stopped, and both ends of the fractured core were sealed. Thereafter, the fracture was completely healed at 70 °C, after which the formation water was continually injected into the fractured core, and the injection pressure was recorded. The maximum injection pressure when the gel was driven out of the fracture outlet was recorded as the plugging strength of the gel to the fracture. For the plugging tests of porous media, the permeability of the porous media was varied from 5 to 30 μm^2. First, the average diameter of the pores in the porous media with different permeabilities was calculated using the Poiseuille equation, after which the plugging capacity was tested using the same method used for the fracture plugging experiments.

3. Results and discussion

3.1. Synthesis of DN_{SA} hydrogels

In this study, a series of fully physically crosslinked DN self-healing hydrogels with good elongation and strength were prepared, and the preparation process of the hydrogels is shown in Fig. 1. The hydrogels were composed of various physical cross-linking effects: the first physical network of the hydrogels was composed of the hydrophobic association between a hydrophilic monomer (AM) and a hydrophobic monomer (LMA). Owing to the low water solubility of the hydrophobic monomer (LMA), it did not readily form a homogeneous phase with SDS and did not easily pass through the continuous aqueous phase into the interior of the micelles. Studies have demonstrated that the presence of a strong electrolyte (NaCl) enables SDS form worm-like micelles, thus significantly increasing the solubility of LMA and the formation of polymerizable micelles, which in turn co-polymerize with AM to form hydrophobic associative networks with good self-healing properties. The second physical network of the hydrogels was composed of the carboxyl group on SA structure and the trivalent Fe^{3+} ion-forming ionic bond (Li X. et al., 2019). In addition, hydrogen bonds were present between SA and AM, which increased the density of the network structure.

In this study, variable temperature FTIR analysis of the DN_{SA}-2 hydrogels was performed from 25 to 250 °C. The peak positions and intensities of the peaks varied slightly at different temperatures (Fig. 2a), in which the IR spectra obtained at 25 °C were used as the benchmark. Peaks attributed to the N–H stretching vibration in PAAm, the O–H stretching vibration in the hydroxyl group of SA, and O–H stretching vibration in the adsorbed water of the sample were observed in the FTIR spectra of the samples. In addition, the peaks at 2930 and 2855 cm^{-1} were attributed to the symmetric and asymmetric C–H stretching vibrations of methylene group, respectively, and the peak at 2785 cm^{-1} was attributed to the C–H stretching vibration in the hypomethyl group. Further, a broad peak was observed at 1674 cm^{-1}, which is a superposition of several peaks, including the C═O stretching vibration of the carbonyl group in the amide structure, C═O stretching vibration of the carbonyl group in SA, and the C═O stretching vibration of the carbonyl group in SA. The absorption peak at 1452 cm^{-1} was attributed to the C–H bending vibration in the carbon skeleton, whereas the adjacent peak at 1415 cm^{-1} was attributed to the C–N stretching vibration in the amide structure. The peaks at 1353 and 1317 cm^{-1} were attributed to the C–H bending vibration and C–H stretching vibration in the carbon skeleton, respectively. Further, the signal overlap around 1218 cm^{-1} was significant and may be attributed to the N–H swaying vibration in the amide. In addition, a spike was observed at 1115 cm^{-1}, which was attributed to the C–O stretching vibrations in SA. The longitudinal view of the FTIR spectra obtained at different temperatures revealed that the peaks attributed to N–H and O–H stretching vibrations at 3451 cm^{-1} narrowed with increasing temperature (Fig. 2b). This could be attributed to the disruption of hydrogen bonding owing to high temperature and the change in the state of hydroxyl groups from the conjoined state to the free state, confirming the presence of a large number of hydrogen bonding interactions in this gel. In addition, a red-shifting of the peaks at 1674 to 1650 cm^{-1} was observed, which was attributed to the disruption of the hydrogen bond between C═O···H–O–. These FTIR results verified the existence of strong hydrogen bonding interactions between the structures of PAAm and SA and the close physical bonding of the components.

The SN-1, DN_{SA}-1, DN_{SA}-2, DN_{SA}-3, and DN_{SA}-4 hydrogel samples were investigated using SEM, and the SEM images are shown in Fig. 3. Huge pores were observed in the SN-1 sample (Fig. 3a) and the size of the pores in the gel drastically reduced after the addition of SA (Fig. 3b). In addition, the number of pores in the hydrogel decreased with an increase in the SA concentration (i.e., smoother surface under the electron microscope; Fig. 3b–e). Further, the SEM results revealed that the SN-1 sample exhibited only a single-layer network structure, which was not densely cross-linked. In addition, the cross-linking degree increased significantly with the appearance of a second network of SA cross-linked with Fe^{3+} ions, indicating that the cross-linking degree of the gels increased with increasing SA concentration, and that the cross-linking degree tended to correlate with the strength of the hydrogels.

3.2. Mechanical properties of the DN_{SA} hydrogels

The hydrogel samples exhibited good elongation and strength. To visualize the mechanical properties of the hydrogels, different shapes of the hydrogels were prepared, and photographs of the DN_{SA}-2 gel samples were obtained. Fig. 4a shows the compression

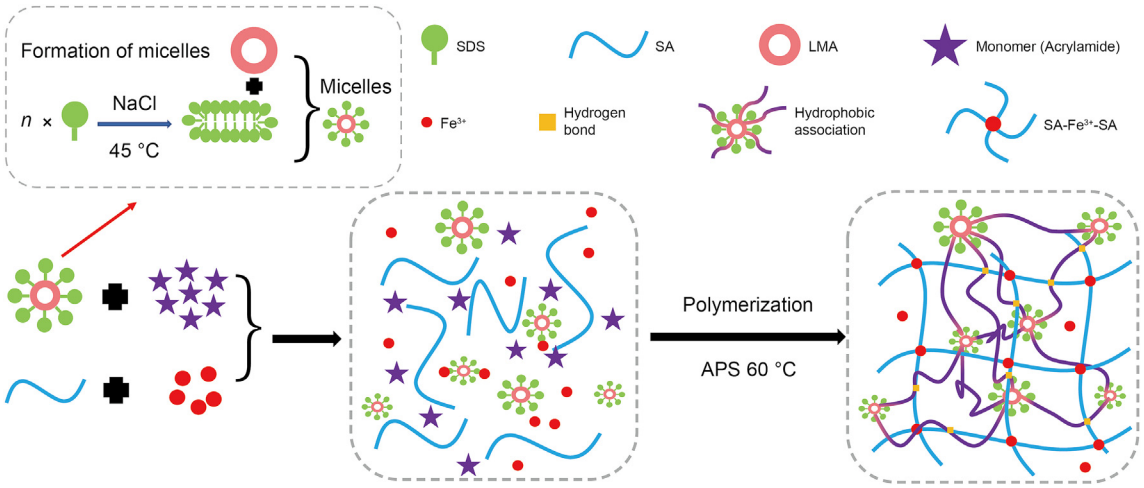

Fig. 1. Synthesis and network structure schematic diagrams of DN_{SA} hydrogels.

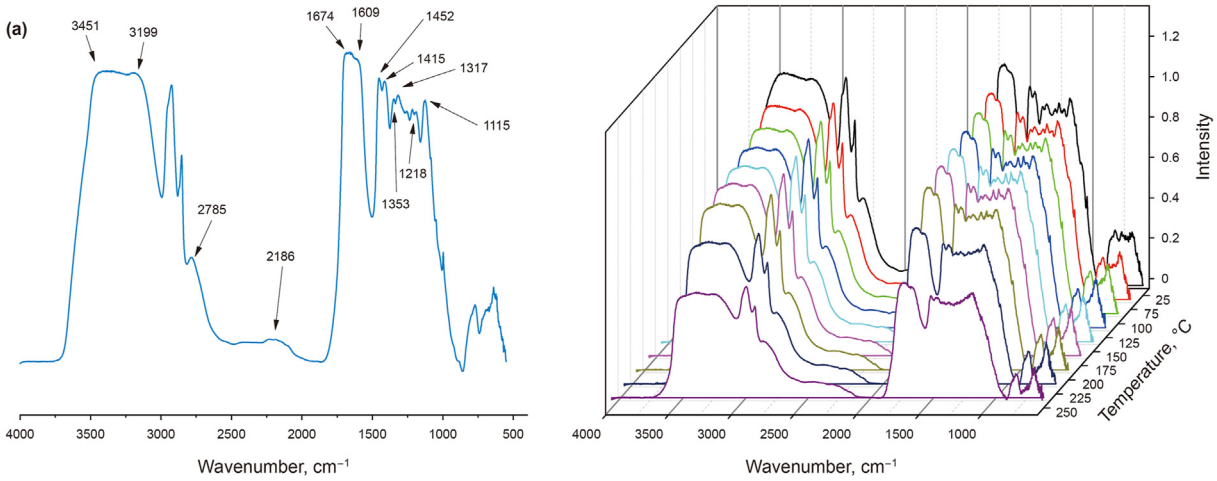

Fig. 2. FTIR spectra of hydrogels. (**a**) FTIR spectrum of DN_{SA}-2 hydrogel at 25 °C; (**b**) Variable temperature FTIR spectra of DN_{SA}-2 hydrogel at 25–250 °C.

process of the hydrogel. The hydrogel exhibited good deformability, and the cylindrical hydrogel can almost completely return to its original shape after compression. After stretching the circular hydrogel in both the transverse and longitudinal directions, the hydrogel did not break, and it formed a thin film, indicating the good toughness of the hydrogel (Fig. 4b). In addition, we prepared a cylindrical hydrogel strip using a 2-mL syringe, and this hydrogel could easily pull up a weight of up to 3 kg without breaking, and the strip could be folded and stretched to 10 times the size of its original length without breaking (Fig. 4c).

As a good performance gel plugging agent, it needs to have a certain strength and deformability to achieve a good plugging of different types of strata. The strength of the gel can be reflected by the fracture stress, while the deformability of the gel can be reflected by the elongation. The fracture stress and elongation of hydrogels are two of the most important parameters in hydrogel applications. Studies have demonstrated that SA exhibits some rigidity and can significantly affect the mechanical properties of hydrogels, so we investigated the effect of different SA concentrations on the mechanical properties of fully physically cross-linked DN hydrogels. Fig. 5 shows typical stress–strain curves and Young's modulus toughness histograms of the hydrogel samples. The SN-1 hydrogel exhibited a good elongation at break (1704%); however, owing to the presence of only a hydrophobically joined monolayer network structure in the hydrogel, the density of the cross-linking degree was insufficient, which resulted in a weak hydrogel strength (0.14 MPa stress at break). Compared to the single network hydrogels, the DN_{SA} hydrogels exhibited significantly increased fracture stress, with DN_{SA}-4 hydrogels achieving a fracture stress of 0.67 MPa, which exceeded that of several previously reported DN hydrogels based on hydrophobic linkages and ionic bonds, such as PAA/AMPS/ST hydrogel (Shang et al., 2021) and cationic guar/acrylic (Jing et al., 2021) double network hydrogel. In addition, the fracture stress of DN_{SA}-4 hydrogel was 4.8 times higher than that of SN-1 hydrogel, which can be attributed to an increase in the formation of cross-linking sites with Fe^{3+} ions with an increase in SA content. Moreover, as the degree of intermolecular crosslinking of hydrogels increased, the density of the network structure of the hydrogels increased, thus increasing the force required to destroy the structure of hydrogels. The increase in the density of the network resulted in an increase in Young's modulus with an increase in the SA content. In addition, the elongation at break of the DN_{SA}-1 hydrogels (2727%) was significantly higher than that of the SN-1 hydrogels (1704%), indicating that there was a synergistic effect between the second heavy network formed by the cross-linking of SA and Fe^{3+} ions and the first heavy network,

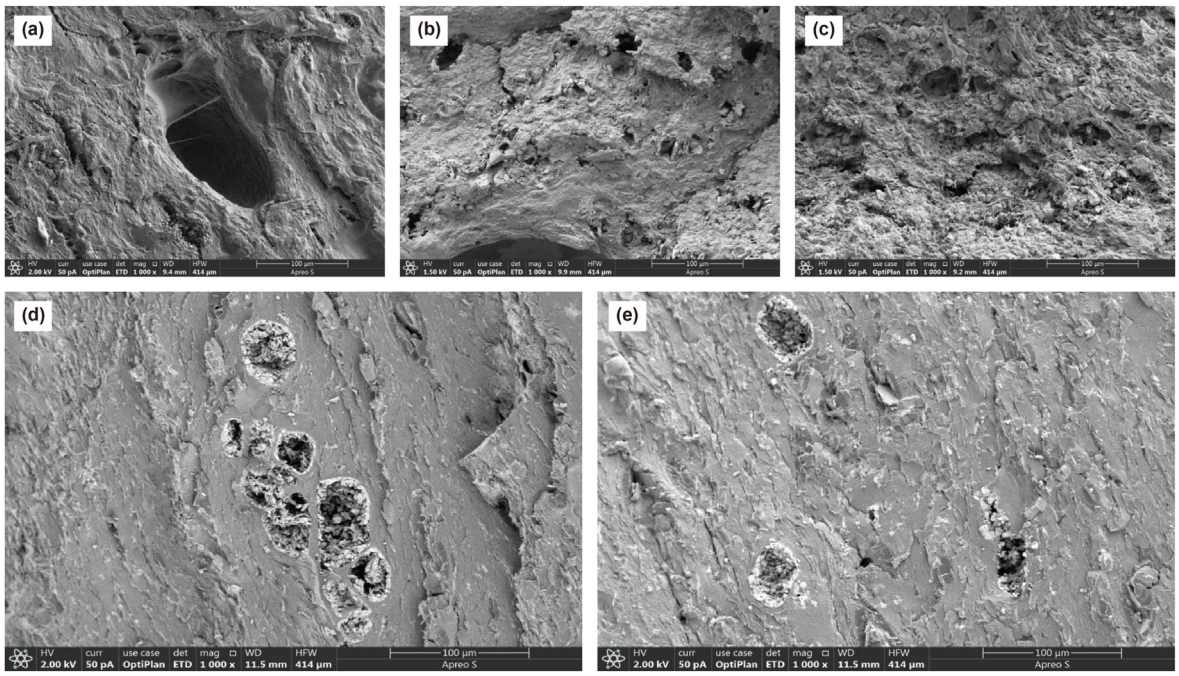

Fig. 3. SEM images of (**a**) SN-1, (**b**) DN_{SA}-1, (**c**) DN_{SA}-2, (**d**) DN_{SA}-3, and (**e**) DN_{SA}-4 hydrogels.

which optimized the performance of the gels. However, as the SA content of the DN_{SA} hydrogels increased, their elongation at break decreased, indicating that the increased degree of crosslinking exhibited a negative effect on the elongation at break. As SA exhibits a positive effect on the fracture stress of the hydrogels and a negative effect on the elongation at break of the hydrogels, the toughness of the hydrogel exhibited an interesting phenomenon, that is, the toughness first increased and then decreased with increasing SA content. Therefore, we concluded that there was an optimum crosslinking concentration for the hydrogels, and that excessive cross-linking was not conducive for optimizing the mechanical properties of the hydrogels. As the DN_{SA}-2 was the most ductile hydrogel sample with a toughness of 7069.29 kJ/m^3, which was greater than that of several chemically cross-linked hydrogels, the DN_{SA}-2 sample was selected for further studies.

To clarify the energy dissipation mechanism of hydrogels, the DN_{SA}-2 hydrogel was subjected to loading–unloading tests at strains of 200%, 400%, 600%, 800%, and 1000%. The hysteresis loop of the loading–unloading curve of the DNSA-2 hydrogel becomes larger (Fig. 6a), and the dissipated energy increased significantly (from 27 to 634.43 kJ/m^3) with an increase in the strain (Fig. 6b), indicating that the damage to the network structure in the hydrogel increased with increasing strain, and the recovery from this damage within a short time was difficult (Tuncaboylu et al., 2012). This phenomenon may be attributed to the destruction of some micellar centers of the hydrophobic association, and the long time required to recover during the loading–unloading process. In addition, we observed an overlap between adjacent strain hysteresis loops, and the size of the overlap region positively correlated with the strain size. The overlap of the hysteresis loops indicated that the sample exhibited good self-healing ability.

Next, we performed loading–unloading tests on the DN_{SA}-2 hydrogels at a fixed strain (1000% strain), and the energy dissipation capability of the hydrogel was observed to increase with an increase in the hysteresis loop of the hydrogel. Fig. 6c and d shows the test results of five consecutive interval-free loading–unloading tests. The stress–strain curve of the hydrogel exhibited a very large hysteresis loop with a dissipated energy of up to 634.43 kJ/m^3 in the first loading–unloading test, which was attributed to the presence of a stable network structure in the hydrogel. However, in the subsequent second loading–unloading curve, the dissipated energy of the hydrogel decreased significantly, indicating that the hydrogel could not immediately recover from the internal damage possibly because of the alignment of the polymer chains in the stress direction and the difficulties in the immediate recovery of the hydrophobic linkage after disruption. However, during the subsequent 3–5 loading–unloading cycles (dissipated energy of approximately 75 kJ/m^3), the hysteresis loops of the hydrogels remained almost stable, which may be attributed to the presence of ionic bonds acting as reversible sacrificial bonds in the hydrogel network, with the Fe^{3+} ions being pulled out during loading and the hydrogel immediately returning to its original position at the crosslinking site during unloading, with the hydrogel immediately recovering its original properties. Further, the loading–unloading tests were conducted on the DN_{SA}-2 hydrogel at different time intervals, and the stress–strain curves (Fig. 6e) and dissipated energy (Fig. 6f) indicated that the hysteresis loops of the hydrogel increased continuously with increasing time, and there was only a small increase in the hysteresis loops of the hydrogel after 1 min, indicating the difficulties of the hydrogel in recovering the conformational phase transformation of the polymer chain due to stress within a short time. However, with an increase in the recovery time, the recovery rate of the hydrogel was 67.58% after 4 h of recovery, indicating the good ability of the hydrogel to recover its original properties, which was attributed to the hydrophobic bonding and the excellent reversibility of ionic bonds. DN_{SA}-2 hydrogels also exhibit excellent notch insensitivity and compression resistance (See Fig. S1 and Fig. S2 for details in Supplementary Material).

3.3. Rheological properties of the DN_{SA} hydrogels

Hydrogels are typically viscoelastic materials, and storage modulus (G') and loss modulus (G'') are the two most important

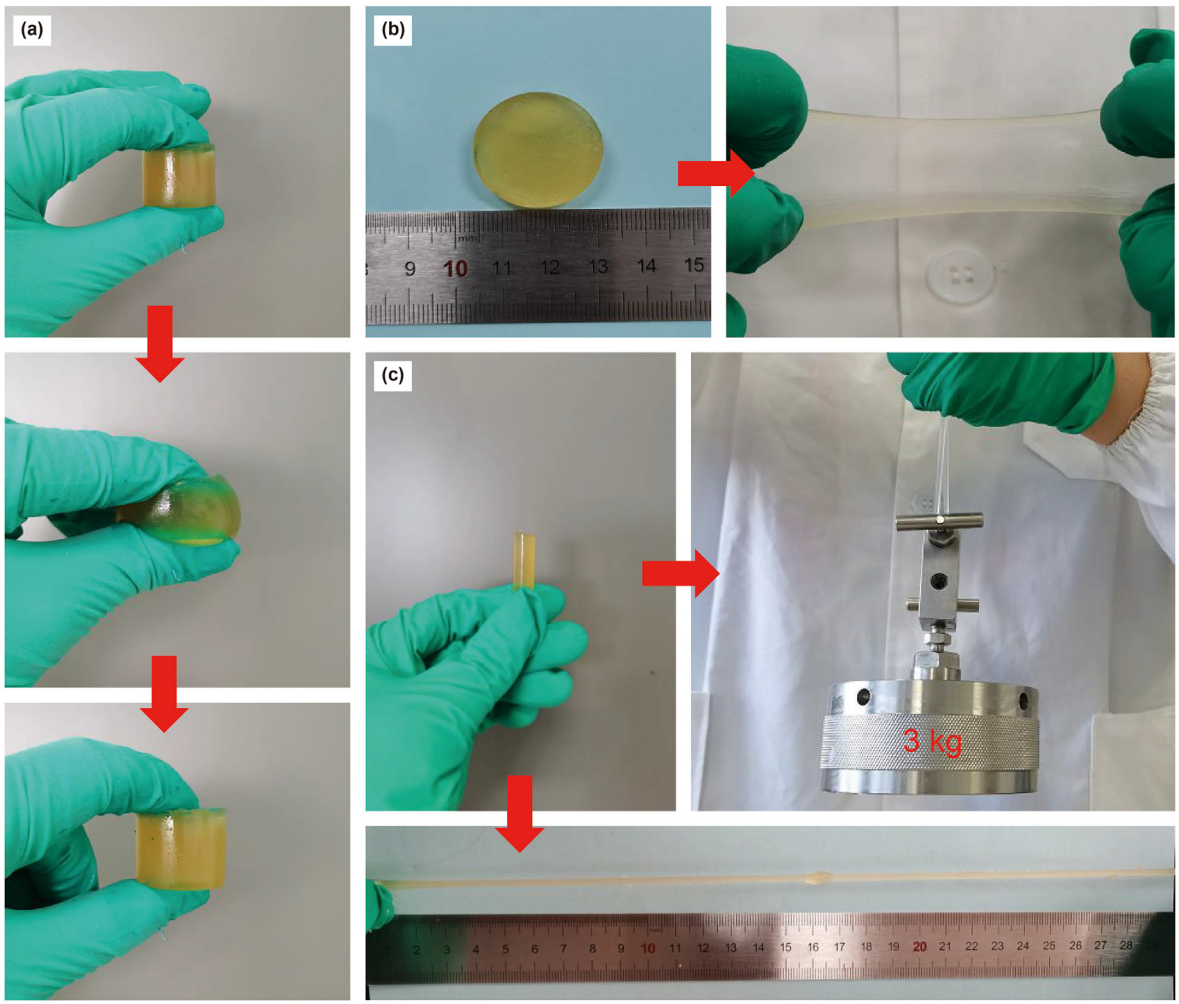

Fig. 4. Exhibition of DN_{SA}-2 hydrogel. (**a**) Columnar hydrogel compression process; (**b**) Stretching process of round sheet hydrogel; (**c**) Hydrogel load-bearing process and bending and stretching process.

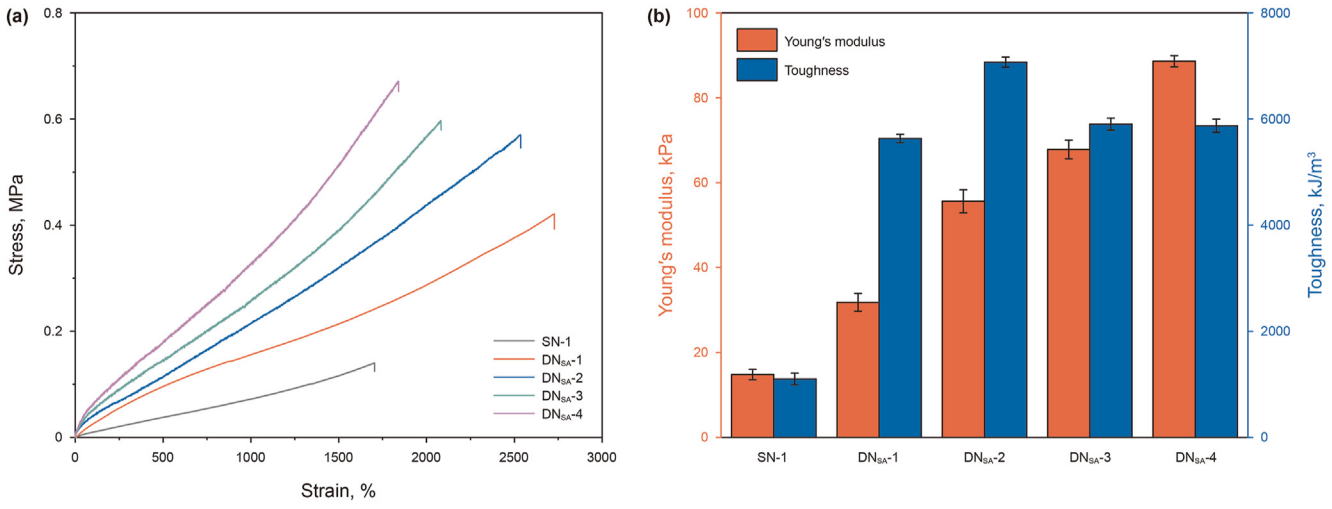

Fig. 5. Mechanical properties of SN-1 hydrogel and DN_{SA} hydrogels. (**a**) The tensile strain–stress curves; (**b**) Elastic modulus and toughness.

parameters for characterizing the rheological properties of hydrogels. The rheological properties of gel materials are affected by changes in strain, frequency, and other conditions. First, we performed strain sweeps on the five samples with a change in the strain from 0.1% to 1000% to determine the linear viscoelastic zone (where the stability of the gel modulus was maintained with a

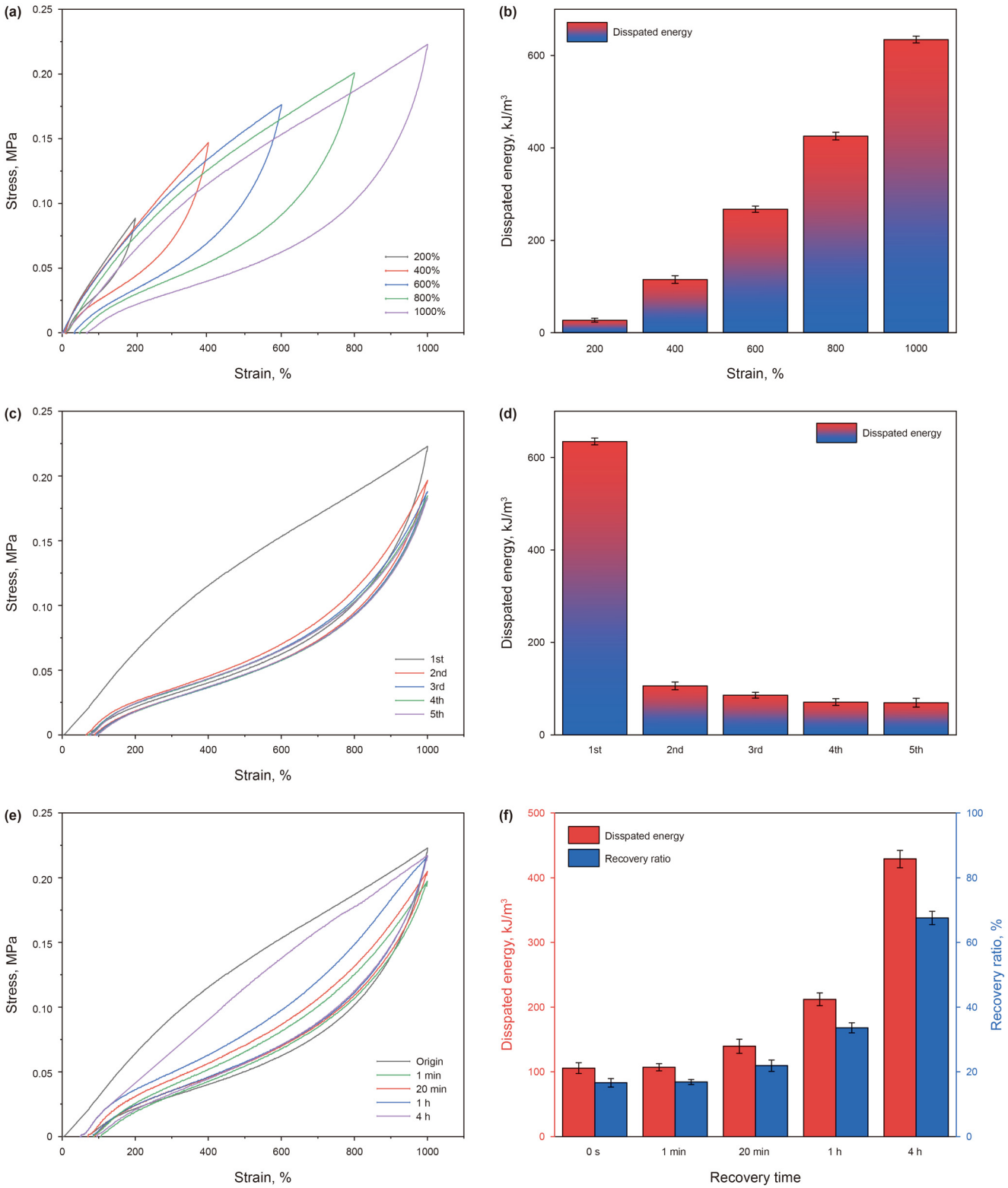

Fig. 6. (**a**) Loading–unloading tensile curves and (**b**) dissipated energy of DN_{SA}-2 hydrogels at different stretch ratios. (**c**) Five successive loading–unloading cycles and (**d**) dissipated energy of DN_{SA}-2 hydrogels at a fix strain of 1000%. (**e**) Five loading–unloading cycles and (**f**) dissipated energy and recovery rate of DN_{SA}-2 hydrogels after five different time rests (strain: 1000%).

change in strain) and the gel transition point (the intersection of G' and G'') of the hydrogels. Studies (Fig. 7) have demonstrated that the transition point appears earlier with an increase in the density of a gel structure. The SN-1 sample did not display a gel transition point within the scan range, indicating the relatively loose density of the crosslinking within the SN-1 single network gel, whereas the

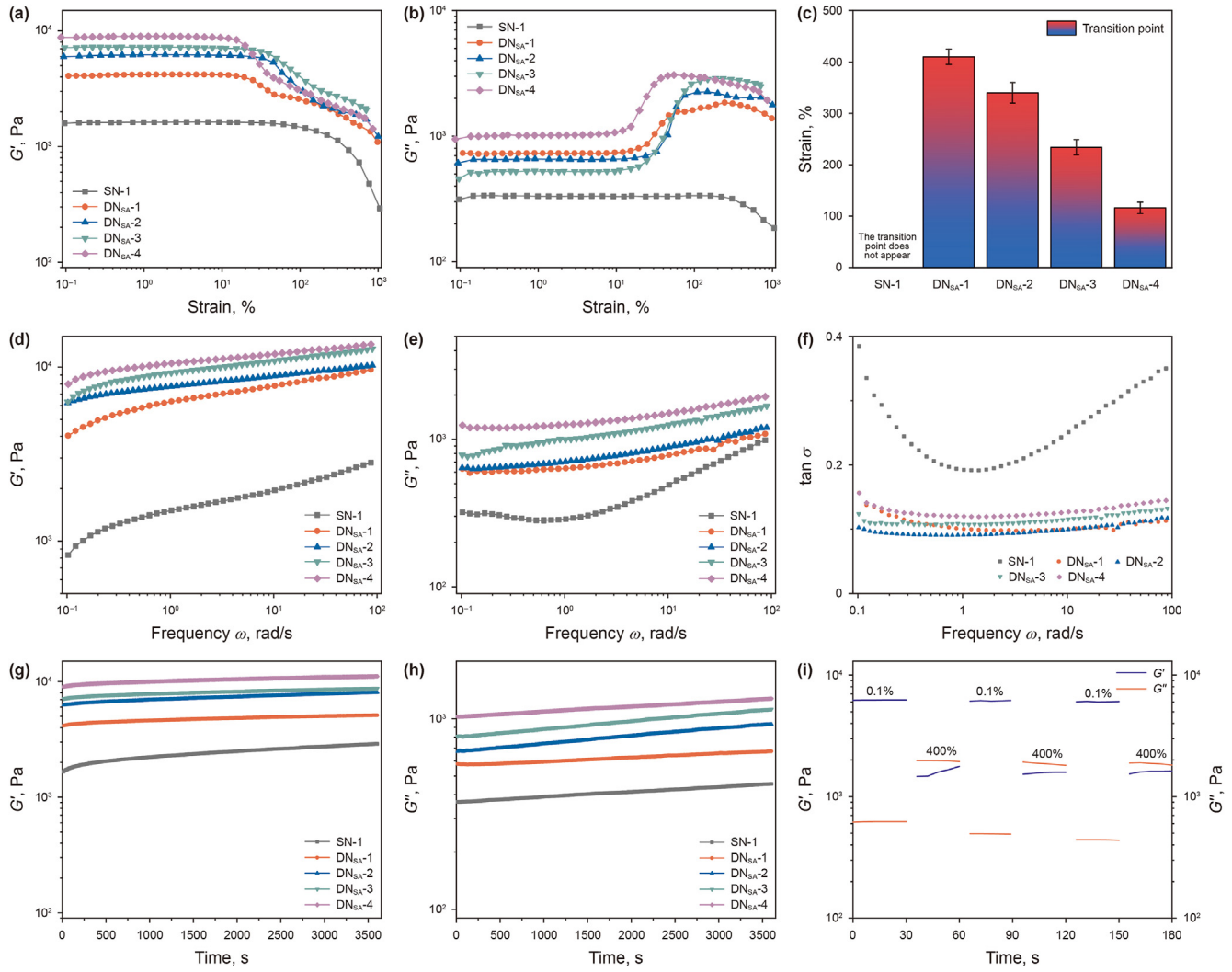

Fig. 7. Rheology tests (25 °C). (**a**) Storage modulus G' and (**b**) loss modulus G'' of the hydrogels under an angular strain sweep; (**c**) Transition point of hydrogels; (**d**) Storage modulus G' and (**e**) loss modulus G'' of the hydrogels under an a frequency sweep; (**f**) The tan σ of hydrogels under a frequency sweep (angular frequency $\omega = 0.1$–100 rad/s, strain of 1%); (**g**) Storage modulus G' and (**h**) loss modulus G'' of the hydrogels under a time sweep; (**i**) Step–strain test of DN_{SA}-2 hydrogel at a fixed frequency of 6.28 rad/s (1% or 100% of strain was applied).

onset of the transition point of the DN_{SA} hydrogel series decreased with an increase in the SA content (Fig. 7c). This indicates that crosslinking between SA and Fe^{3+} ions and the crosslinking density of the gel network increased as the SA content increased, which is consistent with our aforementioned conclusion.

Next, the five hydrogel samples were tested with frequency sweeps from 0.1 to 100 rad/s at a fixed strain of 1% (within the linear viscoelastic region). Over the entire frequency sweep range, the G' of the five samples was consistently higher than the G'' (Fig. 7d and e), and the gels maintained their elasticity, and the same results were obtained after sweeping for 1 h, indicating the good stability of the gels (Fig. 7g and h). In addition, the modulus of elasticity and loss modulus of the hydrogels increased with increasing SA content, and the viscoelastic modulus of the five gel samples exhibited a frequency dependence, wherein the viscoelastic modulus of the gel increased with increasing frequency, which is consistent with the findings of Lin et al. (2021). This can be attributed to the difficulties in the immediate rearrangement of the macromolecular chains present in the gel samples with increasing frequency, and the hardening of the hydrogels. The tan σ (tan $\sigma = G''/G'$) of the gels was calculated, and the results revealed that the gel behaved like an elastic material when tan $\sigma < 1$, and the elasticity of the gel increased with a decrease in the tan σ value, and its recovery ability was also enhanced. Although the DN_{SA}-2 hydrogel did not exhibit the large G' values among the five samples, it exhibited the smallest tan σ value (between 0.09 and 0.12), indicating the good recovery ability of the sample (Fig. 7f).

The transition point of the DN_{SA}-2 hydrogel occurred at 340%, so time sweeps of the hydrogel were performed using strains of 0.1% and 400% (time interval 30 s). The gel changed from a gel state to a sol-gel state at a strain of 400%, indicating that the internal structure of the hydrogel sample was damaged (Fig. 7i); however, when the strain was changed to 0.1%, the hydrogel behaved like a gel again with slight change in modulus, further confirming the excellent recovery ability of the sample.

3.4. Self-healing properties of DN_{SA} hydrogels

The prepared DN hydrogels were composed of both hydrophobic linkage and ionic bonding. Both the hydrophobic linkage and ionic bonding are physical crosslinking and non-covalent bonds, and exhibit the ability to break and re-crosslink. Tuncaboylu et al.

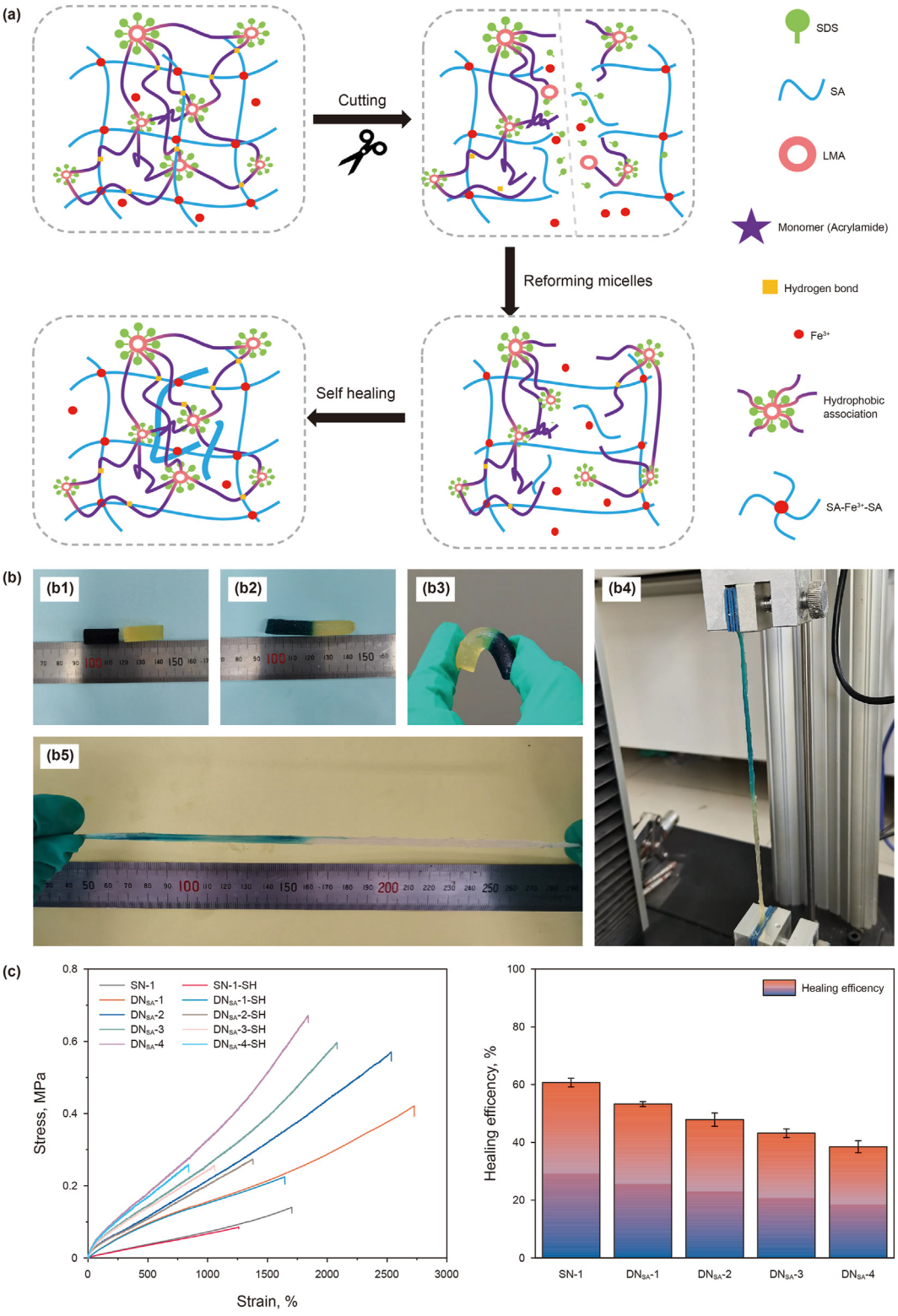

Fig. 8. Self-healing properties of hydrogels. (**a**) Healing mechanism of DN_{SA} hydrogels; (**b**) Physical pictures of DN_{SA}-2 hydrogel before and after healing: (**b1**) two unhealed sections of hydrogel, (**b2**) pictures of hydrogel after healing, (**b3**) bending of hydrogel after healing, (**b4**) tensile test of hydrogel after healing, (**b5**) tensile condition of hydrogel after healing; (**c**) Comparison of stress–strain curves and healing efficiency of SN-1 and DN_{SA} hydrogels before and after healing.

(2011) demonstrated that hydrophobic linkage networks can exhibit excellent healing properties at suitable temperatures, so when the network structure of hydrogels is broken under the action of external forces, the cross-linked structure can be regenerated, which is macroscopically manifested as the self-healing phenomenon of the hydrogels.

The healing mechanism of the hydrogels is shown in Fig. 8a, where the SDS on the gel surface containing the stearyl groups of

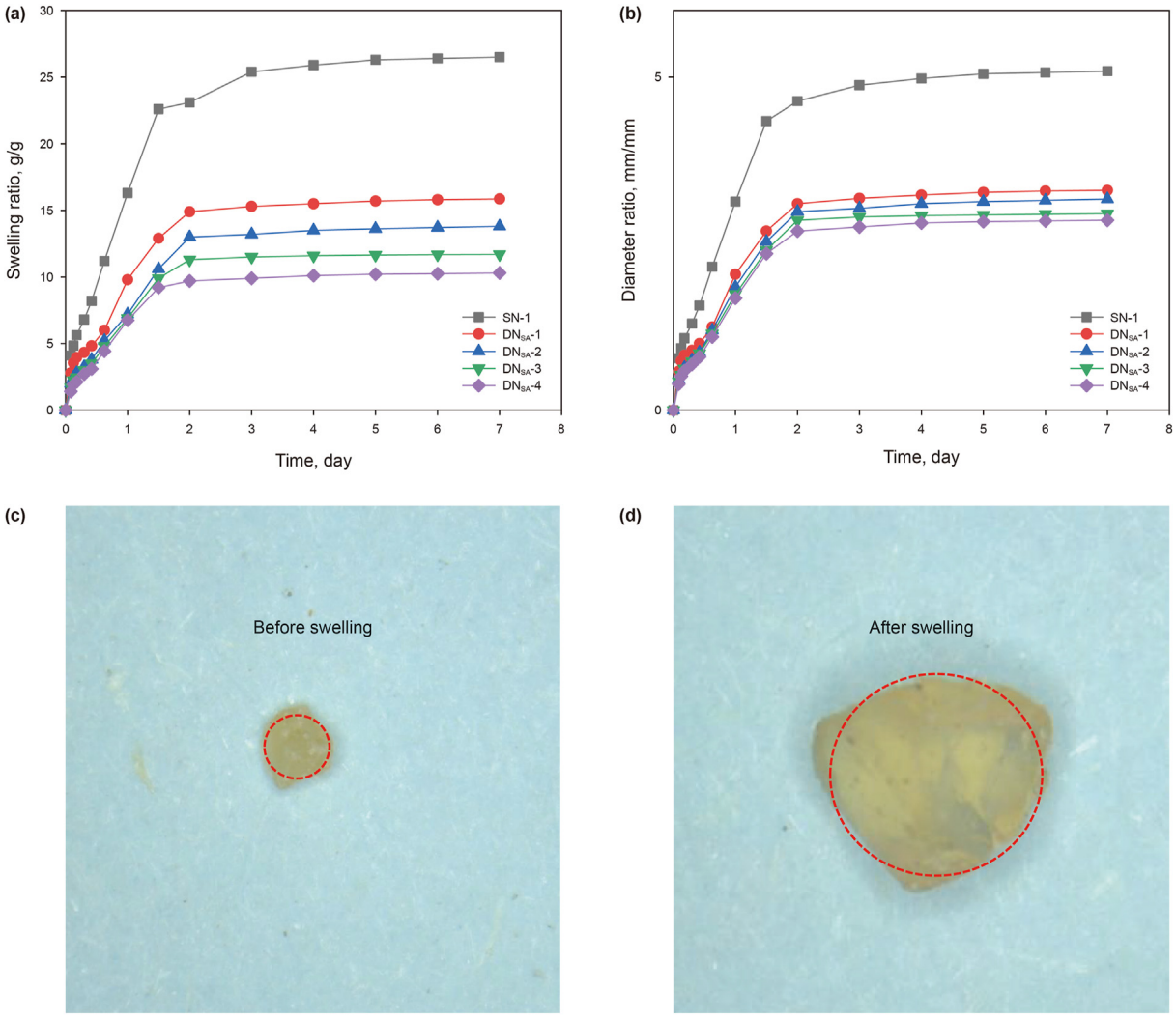

Fig. 9. Swelling of SN-1 and DN_{SA} hydrogels within seven days. (**a**) Mass swelling ratio curve; (**b**) Particle size swelling ratio curve; (**c**) Microscopic image of DN_{SA}-2 gel particles before swelling; (**d**) Microscopic image of DN_{SA}-2 gel particles after swelling.

LMA attached to the side chain of AM to form a new micelle via the interaction of temperature and water molecules on the section, thus forming a new hydrophobic linkage and repairing the cut. The carboxyl groups on the broken SA chain can also be crosslinked with free iron ions again, but SA itself is somewhat rigid, which prevents the complete crosslinking of SA with Fe^{3+} ions after the break, thus hindering the complete healing of the gel. In this study, the ratio of the fracture stress of the healed hydrogels to the fracture stress of the original hydrogels was considered as the healing efficiency of the gels, and the results are shown in Fig. 8b. The hydrogels exhibited a good healing effect, and the presence of cut could hardly be observed on two differently colored hydrogel strips after healing at 70 °C for 12 h. Moreover, the healed samples could withstand bending, stretching, and other operations without being damaged. Fig. 8c shows a physical view of the healing interface of the hydrogel, which almost completely disappeared after healing, demonstrating the excellent self-healing properties of the hydrogel.

Fig. 8c shows stress–strain curves and healing efficiency of the hydrogels after healing. After healing, the hydrogel samples still exhibited a good elongation and strength, and the SN-1 sample exhibited the highest healing efficiency (60.9%), indicating that the healing performance of the hydrogels was mainly dependent on the hydrophobic association. Although the DN_{SA} hydrogels exhibited a good healing performance, their healing efficiency decreased with increasing SA content (53.34%–38.60%). As SA itself exhibits a certain rigidity, the molecular chain density of the hydrogel increased with increasing SA content, and the form of new molecular structure becomes more difficult. Thus, the formation of new crosslinks needs to overcome greater resistance, which shows a decrease in the healing performance on a macro level. Moreover, compared to ionic bonds, hydrophobic association plays a leading role in the healing performance of hydrogels. An increase in the SA content resulted in the generation of more ionic bonds in hydrogels, which resulted in fewer free moving hydrophobic blocks, thus reducing the healing efficiency.

3.5. Plugging performance of the hydrogels

To investigate the plugging performance of the hydrogels, self-healing hydrogel blockers were prepared using granulated hydrogels. The change in the swelling of plugging agents plays a pivotal role in their blocking performance, and the swelling rate curves of the five gel samples were recorded at different times over a period of seven days (Fig. 9a). The slope of the swelling curve is defined as the swelling rate of the hydrogels, and SN-1 hydrogel exhibited the

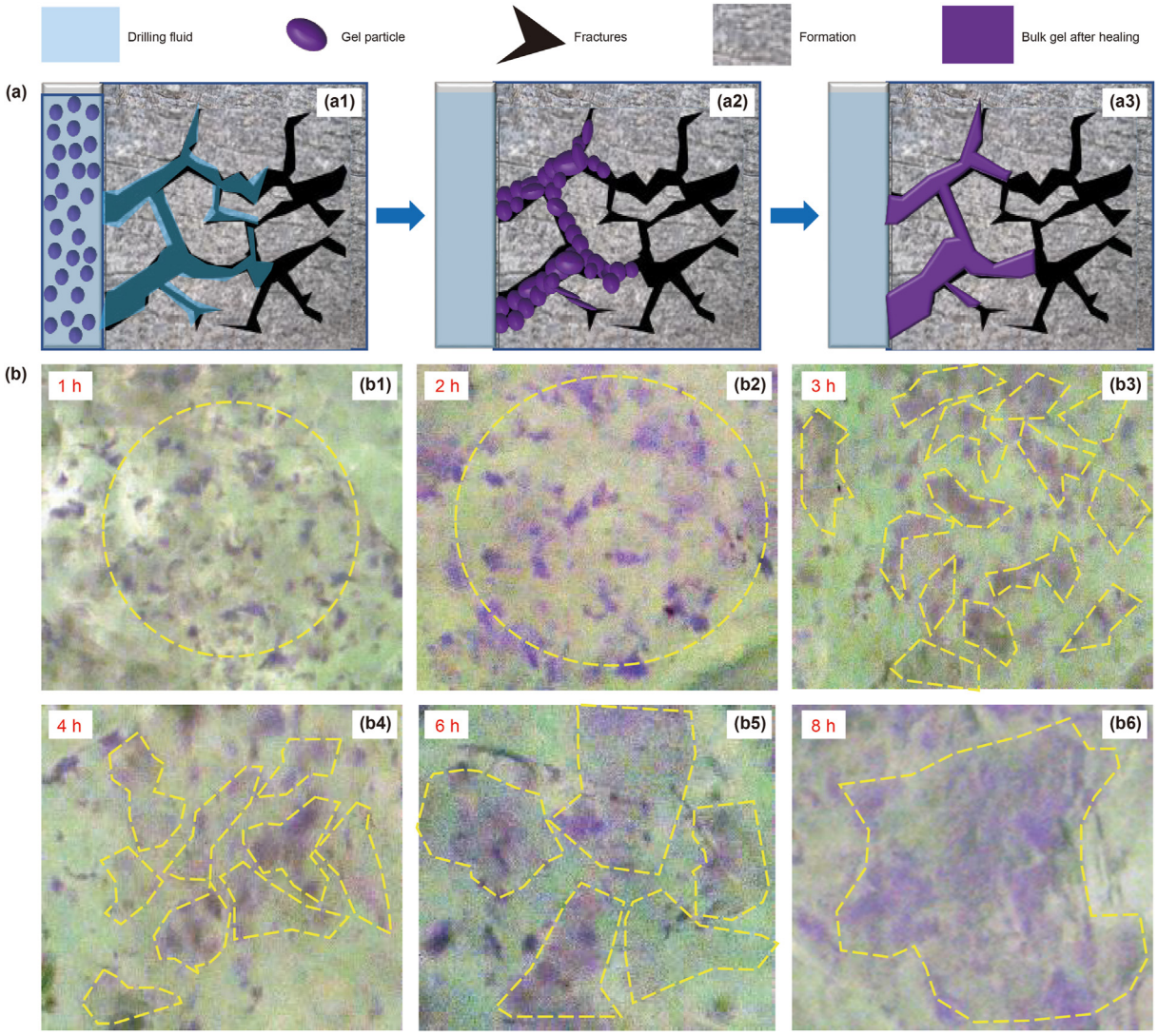

Fig. 10. Schematic diagram and visualization of self-healing hydrogel plugging fractures. (**a**) Diagram of the mechanism of fracture plugging by self-healing hydrogel: (**a**1) gel particles circulate in the wellbore with the drilling fluid, (**a2**) gel particles enter the fracture, (**a3**) gel particles heal in the fracture to become a bulk gel and achieve plugging; (**b**) Microscopic pictures of the fracture plugging process by self-healing hydrogel particles (1–8 h).

fastest swelling rate (maximum slope) and mass swelling rate (mass swelling rate: 26.5) owing to the fact that the SN-1 hydrogels only exhibit a monolayer network of hydrophobic junctions, and the loose lattice structure provided more space for water molecules. As the SA content in the hydrogel increased, the swelling rate of the hydrogels gradually decreased, indicating a reduction in the space for water molecules and an increase in the density of the grid structure within the hydrogel. In addition, the swelling multiplier of the particle size of the hydrogels after swelling at different times was recorded. As shown in Fig. 9b, c, d, the hydrogels exhibit a good swelling multiplier of particle size (>2.8 times). After entering the stratum, they initially stack and then swell, thus compacting each other. The excellent swelling of the hydrogel increased the contact surface between the gel particles, thus increasing their healing efficiency. The plugging mechanism of the self-healing gel particles on fractures is shown in Fig. 10a. After the entry of the self-healing gel particles (3%) into the formation with drilling fluid, the fractures were initially blocked by stacking and bridging. With time, the swelling ratio of the gel particles increased, and the contact between particles increased. The hydrophobic association and the reformation of ionic bond enabled the gel particles heal into a whole gel to achieve high-strength fractures plugging.

After the granulation of the DN_{SA}-2 self-healing hydrogels, according to the "1/2″ bridging theory (Abrams, 1997; Chen et al., 2020), self-healing gel particles with an average particle size of 1.50 mm were selected as plugging agents, the concentration of gel plugging agent is usually 2%–5%. Therefore, we choose the concentration of 3%, and 3% self-healing gel particle dispersion solution was prepared and injected into the fracture model with a fracture width of 3 mm. Fig. 10b shows the morphological changes of the hydrogel particles in the fracture model with time within 8 h, to verify the conjecture of the author on the plugging mechanism of the hydrogel. Within 1 h, the gel particles achieved preliminary stacking in the fracture model, but new micelles were yet to be formed and the gel swelling multiplier was small, so the boundaries between gel particles were distinct. With an increase in time, the swelling ratio of the gel particles increased, and new micelles were partially formed. At 4 h, the gel particles were partially combined, but there were still distinct boundaries between each gel region. At 8 h, the boundary between gel particles almost disappeared, and

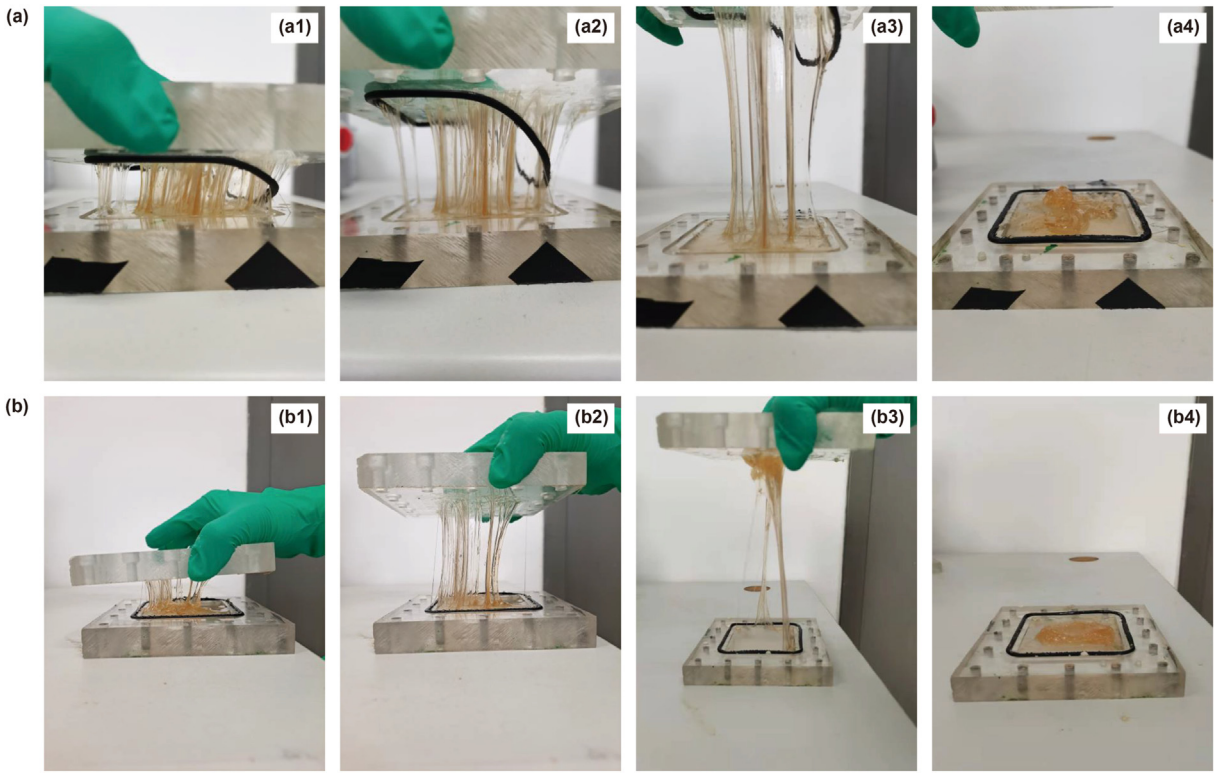

Fig. 11. (**a**) Physical pictures of the stretching of the bulk gel with self-healing gel particles healing for the first time in the fracture; (**b**) Physical pictures of the secondary stretching after healing again.

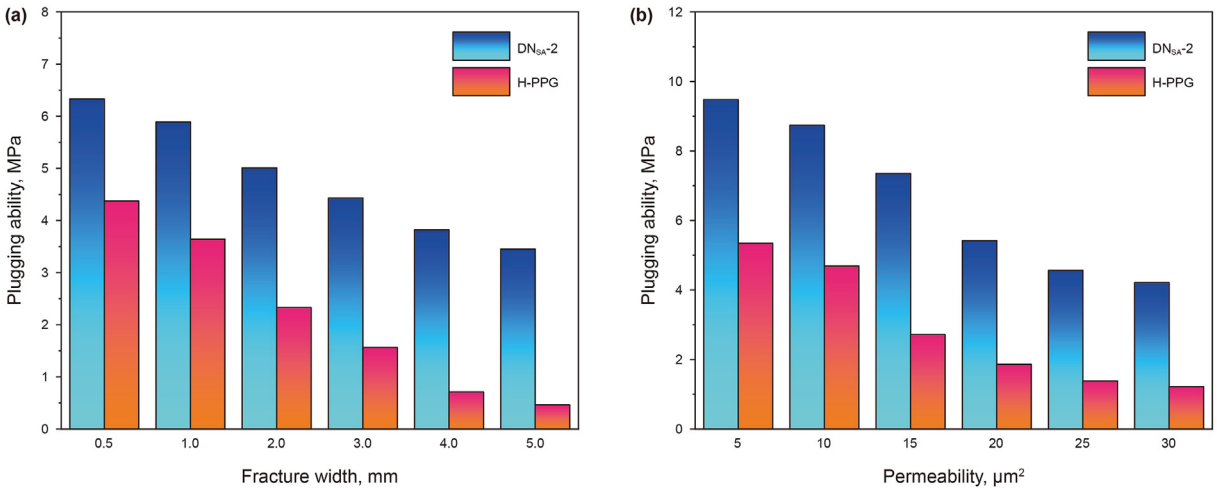

Fig. 12. Plugging effect of self-healing gel particles on fractures with different seam widths and porous media with different permeabilities. (**a**) Plugging effect on fractures with different seam widths; (**b**) Plugging effect on porous media with different permeabilities.

gel particles were re-formed as a whole gel under the hydrophobic association, thus sealing the fractures. After the complete healing of the fractures by the self-healing hydrogel particles, the upper cover of the fracture model was removed and the fractures were observed to be free of free moisture and the self-healing gel formed was strongly adhered to the cover plate and bottom plate of the fracture. As the cover was removed, the gel was stretched (Fig. 11), a phenomenon that suggests an enhancement in the elasticity and resilience of the gel formed by the healing of the self-healing gel particles, which is consistent with the aforementioned healing effect of the self-healing gel in air (Jing et al., 2021). To further investigate its self-healing properties, the pulled hydrogel was repositioned in the fracture model with the upper cover installed, left for 4 h to heal again, after which the cover was removed again and stretched. The hydrogel exhibited good tensile effects, indicating its subsequent healing and formation of a monolithic gel with excellent properties.

To further explore the plugging performance of the DN_{SA}-2 self-healing gel particles, the test method introduced in Section 2.7 was employed to investigate the plugging effect of the self-healing gel particles on porous media with different permeability and fractures of different widths. With an increase in the fracture width, the

plugging ability of both DN_{SA}-2 gel particles and H-PPG to fractures decreased (Fig. 12a). The plugging ability of the DN_{SA}-2 hydrogel particles to fractures with a width of 5 mm was 3.45 MPa. As the plugging ability of the gels was mainly based on the strength of the gels themselves and the cementing ability of the gels with the fracture walls, the cementing ability of the gels with the fracture walls was maintained with an increase in the fracture width, but the healed gels were more likely to be squeezed by the water phase, thus destroying the gels. For H-PPG, as it does not exhibit healing properties, its fracture-sealing effect mainly relied on the accumulation effect between the particles, and the particle accumulation was easily washed out with an increase in the width of the fractures. Therefore, compared to that of DN_{SA}-2, the plugging ability of H-PPG was more sensitive to fracture width, and its plugging ability to a fracture with a width of 5 mm was only 0.46 MPa. Fig. 12b shows that the influence of permeability on the sealing capacity of DN_{SA}-2 gel particles and H-PPG is consistent with that of fractures (i.e., the pore diameter increased and the sealing capacity decreased with an increase in the permeability). The DN_{SA}-2 gel particles exhibited a higher plugging capacity of 4.21 MPa for the porous media with a permeability of 30 μm^2 compared to that of H-PPG (1.22 MPa). The aforementioned experimental results demonstrated the DN_{SA}-2 self-healing gel particles had higher sealing ability to fracture and porous media compared to the commonly used gel particle sealers in the oilfield, which could be attributed to its excellent properties.

4. Conclusions

In this study, DN_{SA}, DN self-healing hydrogels based on hydrophobic association and ionic bonding, were successfully prepared and employed to seal pores and fractures in formations in oil and gas drilling and production engineering. Compared to the single network hydrogels with hydrophobic association, the DN_{SA} hydrogels exhibited good mechanical properties owing to the synergistic effect of the double network, with a fracture stress of 0.67 MPa, a toughness of 7069 kJ/cm^3, and a compressive stress of 16.26 MPa. In addition, owing to its hydrophobic bonding and ionic bonding, which are both non-covalent, the DN_{SA} hydrogels exhibited excellent energy dissipation, notch insensitivity, and excellent healing properties with a maximum healing rate of 53.34%. The DN_{SA}-2 hydrogels with optimum dissipation capacity were granulated into gel particles of different particle sizes and used as plugging agents, which exhibited excellent ability to plug pores and fractures in the formation. The DN_{SA}-2 hydrogel exhibited a plugging capacity of 3.45 MPa for fractures with a width of 5 mm and 4.21 MPa for porous media with a permeability of 30 μm^2, which is significantly higher than those of commonly used plugging agents in the oilfield. The excellent mechanical properties, self-healing ability, and plugging capacity make the DN_{SA} hydrogels ideal candidates for plugging agents in oil and gas drilling and production engineering.

Declaration of competing interest

The authors declare no conflict of interest.

Acknowledgments

This research is financially supported by the National Natural Science Foundation of China (Grant Nos. 52074327 and 51991361).

Appendix A. Supplementary data

Supplementary data to this article can be found online at https://doi.org/10.1016/j.petsci.2022.07.006.

References

Abrams, A., 1997. Mud design to minimize rock impairment due to particle invasion. J. Petrol. Technol. 29 (5), 586–592. https://doi.org/10.2118/5713-PA.
Amir, Z., Said, I.M., Jan, B.M., 2019. In situ organically cross-linked polymer gel for high-temperature reservoir conformance control: a review. Polym. Adv. Technol. 30 (1), 13–39. https://doi.org/10.1002/pat.4455.
Bai, B., Li, L., Liu, Y., et al., 2007. Preformed particle gel for conformance control: factors affecting its properties and applications. SPE Reservoir Eval. Eng. 10, 415–422. https://doi.org/10.2118/89389-PA, 04.
Bai, B., Zhou, J., Liu, Y., et al., 2013. Thermo-dissoluble polymer for in-depth mobility control. Internal Petrol. Technol. Conference. https://doi.org/10.2523/16991-MS.
Bai, Y., Zhang, Q., Sun, J., et al., 2021. Self-healing hydrogels and their action mechanism in oil–gas drilling and development engineering: a systematic review and prospect. J. Nat. Gas Sci. Eng. 96, 104250. https://doi.org/10.1016/j.jngse.2021.104250.
Bazban-Shotorbani, S., Hasani-Sadrabadi, M.M., Karkhaneh, A., et al., 2017. Revisiting structure-property relationship of pH-responsive polymers for drug delivery applications. J. Contr. Release 253, 46–63. https://doi.org/10.1016/j.jconrel.2017.02.021.
Chen, X., Li, Y., Liu, Z.Y., et al., 2020. Investigation on matching relationship and plugging mechanism of self-adaptive micro-gel (SMG) as a profile control and oil displacement agent. Powder Technol. 364, 774–784. https://doi.org/10.1016/j.powtec.2020.02.027.
El-Karsani, K.S.M., Al-Muntasheri, G.A., Sultan, A.S., et al., 2014. Gelation kinetics of PAM/PEI system. J. Therm. Anal. Calorim. 116 (3), 1409–1415. https://doi.org/10.1007/s10973-014-3754-y.
Gaharwar, A.K., Peppas, N.A., Khademhosseini, A., 2014. Nanocomposite hydrogels for biomedical applications. Biotechnol. Bioeng. 111 (3), 441–453. https://doi.org/10.1002/bit.25160.
Gong, J.P., Katsuyama, Y., Kurokawa, T., et al., 2003. Double-network hydrogels with extremely high mechanical strength. Adv. Mater. 15 (14), 1155–1158. https://doi.org/10.1002/adma.200304907.
Hamidi, M., Azadi, A., Rafiei, P., 2008. Hydrogel nanoparticles in drug delivery. Adv. Drug Deliv. Rev. 1638. https://doi.org/10.1016/j.addr.2008.08.002. –49.
Hao, X., Liu, H., Xie, Y., et al., 2013. Thermal-responsive self-healing hydrogel based on hydrophobically modified chitosan and vesicle. Colloid Polym. Sci. 291 (7), 1749–1758. https://doi.org/10.1007/s00396-013-2910-4.
He, P., Guo, R., Hu, K., et al., 2021. Tough and super-stretchable conductive double network hydrogels with multiple sensations and moisture-electric generation. Chem. Eng. J. 414, 128726. https://doi.org/10.1016/j.cej.2021.128726.
Hu, J., Andablo-Reyes, E., Soltanahmadi, S., et al., 2020. Synergistic microgel-reinforced hydrogels as high-performance lubricants. ACS Macro Lett. 9 (12), 1726–1731. https://doi.org/10.1021/acsmacrolett.0c00689.
Jiang, G., Deng, Z., He, Y., et al., 2019. Cross-linked polyacrylamide gel as loss circulation materials for combating lost circulation in high temperature well drilling operation. J. Pet. Sci. Eng. 181, 106250. https://doi.org/10.1016/j.petrol.2019.106250.
Jiang, G., Sun, J., He, Y., et al., 2021. Novel water-based drilling and completion fluid technology to improve wellbore quality during drilling and protect unconventional reservoirs. Engineering. https://doi.org/10.1016/j.eng.2021.11.014, 2021.
Jing, H., Feng, J., Shi, J., et al., 2021. Ultra-stretchable, self-recovering, self-healing cationic guar gum/poly(stearyl methacrylate-co-acrylic acid) hydrogels. Carbohydr. Polym. 256, 117563. https://doi.org/10.1016/j.carbpol.2020.117563.
Kang, W., Kang, X., Lashari, Z.A., et al., 2021. Progress of polymer gels for conformance control in oilfield. Adv. Colloid Interface Sci. 289, 102363. https://doi.org/10.1016/j.cis.2021.102363.
Koetting, M.C., Peters, J.T., Steichen, S.D., et al., 2015. Stimulus-responsive hydrogels: theory, modern advances, and applications. Mater. Sci. Eng. R Rep. 93, 1–49. https://doi.org/10.1016/j.mser.2015.04.001.
Larki, O.A., Apourvari, S.N., Schaffie, M., et al., 2019. A new formulation for lightweight oil well cement slurry using a natural pozzolan. Adv. Geo-Energy Res. 3 (3), 242–249. https://doi.org/10.26804/ager.2019.03.02.
Li, H., Wang, K., Han, X., et al., 2019. Research on heterogeneous compound flooding system based on dispersed particle gel. Adv. Geo-Energy Res. 3 (2), 156–164. https://doi.org/10.26804/ager.2019.02.05.
Li, X., Wang, H., Li, et al., 2018. Dual ionically cross-linked double-network hydrogels with high strength, toughness, swelling resistance, and improved 3D printing processability. ACS Appl. Mater. Interfaces 10 (37), 31198–31207. https://doi.org/10.1021/acsami.8b13038.
Li, X., Zhao, Y., Li, D., et al., 2019. Highly stretchable, tough, and self-recoverable and self-healable dual physically crosslinked hydrogels with synergistic “soft and hard” networks. Polym. Eng. Sci. 59 (1), 145–154. https://doi.org/10.1002/pen.24880.
Lin, Q., Li, H., J, i N., et al., 2021. Self-healing, stretchable, and freezing-resistant hydroxypropyl starch-based double-network hydrogels. Carbohydr. Polym. 251, 116982. https://10.1016/j.carbpol.2020.116982.
Liu, C., Morimoto, N., Jiang, L., et al., 2021. Tough hydrogels with rapid self-reinforcement. Science 372 (6546), 1078–1081. https://doi.org/10.1126/science.aaz6694.
Liu, Y., Liu, Y., Wang, Q., et al., 2020. Doubly dynamic hydrogel formed by combining

boronate ester and acylhydrazone bonds. Polymers 12 (2), 1–15. https://doi.org/10.3390/polym12020487.
Lu, W., Le, X., Zhang, J., et al., 2017. Supramolecular shape memory hydrogels: a new bridge between stimuli-responsive polymers and supramolecular chemistry. Chem. Soc. Rev. 46 (5), 1284–1294. https://doi.org/10.1039/C6CS00754F.
Mansour, A.K., Taleghani, A.D., 2018. Smart loss circulation materials for drilling highly fractured zones. In: SPE/IADC Middle East Drilling Technology Conference and Exhibition. https://doi.org/10.2118/189413-MS.
Merino, S., Martín, C., Kostarelos, K., et al., 2015. Nanocomposite hydrogels: 3D polymer-nanoparticle synergies for on-demand drug delivery. ACS Nano 9 (5), 4686–4697. https://doi.org/10.1021/acsnano.5b01433.
Ouyang, L., Highley, C.B., Rodell, C.B., et al., 2016. 3D printing of shear-thinning hyaluronic acid hydrogels with secondary cross-linking. ACS Biomater. Sci. Eng. 2 (10), 1743–1751. https://doi.org/10.1021/acsbiomaterials.6b00158.
Pu, J., Bai, B., Alhuraishawy, A., et al., 2019. A recrosslinkable preformed particle gel for conformance control in heterogeneous reservoirs containing linear-flow features. SPE J. 24, 1714–1725. https://doi.org/10.2118/191697-PA, 04.
Qu, J., Zhao, X., Ma, P.X., et al., 2017. pH-responsive self-healing injectable hydrogel based on N-carboxyethyl chitosan for hepatocellular carcinoma therapy. Acta Biomater. 58, 168–180. https://doi.org/10.1016/j.actbio.2017.06.001.
Saghafi, H.R., Naderifar, A., Gerami, S., et al., 2016. Improvement in thermo-chemical stability of nanocomposite preformed particle gels for conformance control in harsh oil reservoir conditions. Can. J. Chem. Eng. 94 (10), 1880–1890. https://doi.org/10.1002/cjce.22577.
Scheltjens, G., Diaz, M.M., Brancart, J., et al., 2013. A self-healing polymer network based on reversible covalent bonding. React. Funct. Polym. 73, 413–420. https://doi.org/10.1016/j.reactfunctpolym.2012.06.017.
Shah, L.A., Khan, M., Javed, et al., 2018. Superabsorbent polymer hydrogels with good thermal and mechanical properties for removal of selected heavy metal ions. J. Clean. Prod. 201, 78–87. https://doi.org/10.1016/j.jclepro.2018.08.035.
Shang, X., Wang, Q., Li, J., et al., 2021. Double-network hydrogels with superior self-healing properties using starch reinforcing strategy. Carbohydr. Polym. 257, 117626. https://doi.org/10.1016/j.carbpol.2021.117626.
Soka, S., Sidiq, H., 2022. Sensitivity analysis of parameters affecting nano-polymer solution for water shutoff in carbonate rocks. Adv. Geo-Energy Res. 6 (3), 230–240. https://doi.org/10.46690/ager.2022.03.06.
Sun, J.Y., Zhao, X., Illeperuma, W.R.K., et al., 2012. Highly stretchable and tough hydrogels. Nature 489 (7414), 133–136. https://doi.org/10.1038/nature11409.
Taylor, D.L., Het Panhuis, M., 2016. Self-Healing hydrogels. Adv. Mater. 28 (41), 9060–9093. https://doi.org/10.1002/adma.201601613.
Tuncaboylu, D.C., Sahin, M., Argun, A., et al., 2012. Dynamics and large strain behavior of self-healing hydrogels with and without surfactants. Macromolecules 45 (4), 1991–2000. https://doi.org/10.1021/ma202672y.
Tuncaboylu, D.C., Sari, M., Oppermann, W., et al., 2011. Tough and self-healing hydrogels formed via hydrophobic interactions. Macromolecules 44 (12), 4997–5005. https://doi.org/10.1021/ma200579v.
Unagolla, J.M., Jayasuriya, A.C., 2020. Hydrogel-based 3D bioprinting: a comprehensive review on cell-laden hydrogels, bioink formulations, and future perspectives. Appl. Mater. Today 18, 100479. https://doi.org/10.1016/j.apmt.2019.100479.
Wang, L., Long, Y., Ding, H., et al., 2017. Mechanically robust re-crosslinkable polymeric hydrogels for water management of void space conduits containing reservoirs. Chem. Eng. J. 317, 952–960. https://doi.org/10.1016/j.cej.2017.02.140.
Webber, M.J., Appel, E.A., Meijer, E.W., et al., 2015. Supramolecular biomaterials. Nat. Mater. 15 (1), 3–26. https://doi.org/10.1038/nmat4474.
Xiao, H., Ma, C., Le, X., et al., 2017. A multiple shape memory hydrogel induced by reversible physical interactions at ambient condition. Polymers 9 (4), 1–10. https://doi.org/10.3390/polym9040138.
Xu, Y., Li, Y., Chen, Q., et al., 2018. Injectable and self-healing chitosan hydrogel based on imine bonds: design and therapeutic applications. Int. J. Mol. Sci. 19 (8), 2198. https://doi.org/10.3390/ijms19082198.
Xue, S., Wu, Y., Wang, J., et al., 2018. Boron nitride nanosheets/PNIPAM hydrogels with improved thermo-responsive performance. Materials 11 (7), 1–9. https://doi.org/10.3390/ma11071069.
Yang, C.H., Wang, M.X., Haider, H., et al., 2013. Strengthening alginate/polyacrylamide hydrogels using various multivalent cations. ACS Appl. Mater. Interfaces 5 (21), 10418–10422. https://doi.org/10.1021/am403966x.
Yu, C., Wang, C.F., Chen, S., 2014. Robust self-healing host-guest gels from magnetocaloric radical polymerization. Adv. Funct. Mater. 24 (9), 1235–1242. https://doi.org/10.1002/adfm.201302058.
Yuan, J., Lei, X., Yi, C., et al., 2022. 3D-printed hierarchical porous cellulose/alginate/carbon black hydrogel for high-efficiency solar steam generation. Chem. Eng. J. 430 (P2), 132765. https://doi.org/10.1016/j.cej.2021.132765.
Zhang, H.J., Sun, T.L., Zhang, A.K., et al., 2016. Tough physical double-network hydrogels based on amphiphilic triblock copolymers. Adv. Mater. 28 (24), 4884–4890. https://doi.org/10.1002/adma.201600466.
Zhang, Z., Tang, L., Chen, C., et al., 2021. Liquid metal-created macroporous composite hydrogels with self-healing ability and multiple sensations as artificial flexible sensors. J. Mater. Chem. A. Royal Society of Chemistry 9 (2), 875–883. https://doi.org/10.1039/d0ta09730f.
Zhao, D., Feng, M., Zhang, L., et al., 2021. Facile synthesis of self-healing and layered sodium alginate/polyacrylamide hydrogel promoted by dynamic hydrogen bond. Carbohydr. Polym. 256 (5), 117580. https://doi.org/10.1016/j.carbpol.2020.117580.
Zheng, C., Huang, Z., 2015. Microgel reinforced composite hydrogels with pH-responsive, self-healing properties. Colloids Surfaces A Physicochem. Eng. Asp. 468, 327–332. https://doi.org/10.1016/j.colsurfa.2014.12.060.
Zhong, M., Liu, X.Y., Shi, F.K., et al., 2015. Self-healable, tough and highly stretchable ionic nanocomposite physical hydrogels. Soft Matter. Royal Soc. Chem. 11 (21), 4235–4241. https://doi.org/10.1039/c5sm00493d.